Pharmaceutical Research, Vol. 24, No. 12, December 2007 (© 2007)
DOI: 10.1007/s11095-007-9436-8

Research Paper

Chemical Groups that Adhere to the Surfaces of Living Malignant Cells

Cathy E. McNamee,[1,5] Yuki Aso,[2] Shinpei Yamamoto,[3] Yoshinobu Fukumori,[4] Hideki Ichikawa,[4] and Ko Higashitani[2]

Received April 2, 2007; accepted August 8, 2007; published online September 12, 2007

Purpose. We determined the adhesion of particles with phenyl, carboxylic acid (*COOH*), amine, dialkyl phosphonate, ester, and hydroxyl groups to malignant and nonmalignant cells, in order to better design drug delivery systems (DDS) for malignant cells.
Methods. Living mouse melanoma skin (B16F10) and noncancerous mouse fibroblast (L929) cells, and an Atomic Force Microscope were used to determine the adhesion strengths.
Results. The measurement of the particles against B16F10 cells showed that *COOH* had the highest average maximum adhesion force ($<F_{admax}>$) and a large standard deviation (*std*), and phenyl had the lowest $<F_{admax}>$ and a lower *std*. The high $<F_{admax}>$ and *std* suggested that *COOH* was binding the strongest to malignant cells, and to groups overexpressed on malignant cells. In the case of L929 cells, $<F_{admax}>$ of phenyl and *COOH* were higher and lower, respectively, than those of the B16F10 cells. Additionally, Phenyl and *COOH* gave a lower *std* than that for the B16F10 cells. These results suggest that the lower binding of *COOH* to the nonmalignant cells was due to the lower number of groups that were overexpressed in the malignant cells.
Conclusions. Our results suggest that *COOH* is the best group for malignant cell targeting DDS systems.

KEY WORDS: Atomic Force Microscope colloid probe technique; B16F10 cells; L929 cells; polystyrene; silane coupling agents.

INTRODUCTION

An efficient drug delivery system (DDS) administers an accurate amount of the drug to melanoma cells at a preprogrammed rate and at concentrations required for effective treatment (1). In general, DDS carriers have a core, shell, and a particular surface structure (2). The core predominately controls the size of the carrier (2), effectively determining which blood capillaries it may traverse. The core also generally contains the anticancer drug. The shell is physically or chemically bound to the core, and acts as the base to which the surface molecules may bind (2). The molecules used on the surface of the DDS carrier may control the circulation time of the carrier, and the sites to which the carrier may bind. For example, the circulation time of a carrier has been reported to be increased, when a polymer with a larger molecular weight is used (3,4). The possibility of an adhesion of the carrier to a particular site may be controlled by the chemical functionality groups on the surface of the carrier, where groups that may specifically or nonspecifically adhere to a melanoma cell may cause the DDS carrier to bind predominately to the melanoma cell (5,6). Although we somewhat understand which particle sizes may transverse only the blood capillaries of malignant cells (2), we still do not know well which fundamental chemical groups show the highest adhesion ability and selectivity to melanoma cells. Without this information, it is difficult to design an efficient DDS carrier system.

Up to now, researchers have often been screening a large number of surfactants and polymers in the hope of finding a material that selectively binds to a malignant cell (1). However, this method is both costly and time consuming. Additionally, assuming a material is found that shows some adhesion to a melanoma cell, the fact that each polymer and surfactant commonly used in DDS carriers often contains more than one functional group makes it difficult to determine which groups are contributing to this adhesion. This information is however vital in designing an effective DDS that shows specificity only to malignant cells. We may determine which functional groups show the best adhesion to the surface of a melanoma cell by measuring the adhesion of a single functional group to the surface of a living melanoma cell. This may be achieved by modifying silica particles with silane coupling agents that possess a terminal chemical functional group.

[1] Max Planck Institute for Polymer Research, 55128 Mainz, Germany.
[2] Dept. Chem. Eng., Kyoto University, Katsura, Kyoto, 615-8510, Japan.
[3] Institute for Chemical Research, Kyoto University, Gokasho, Uji, Kyoto, 611-0011, Japan.
[4] Faculty of Pharmaceutical Sciences and Cooperative Research Center of Life Sciences, Kobe Gakuin University, Kobe, 650-8586, Japan.
[5] To whom correspondence should be addressed. (e-mail: mcnamee@mpip-mainz.mpg.de)

Some promising DDS carriers include colloids or surfactant self-assembled objects (7,8), microemulsions (9), liposomes (10,11), monoclonal antibodies (12), and polymer gels (13). Some polymers that are often used in drug delivery as they are biodegradable and appear to show a high adhering possibility to malignant cells include poly(ethylene terephalate) (14), poly(tartronic acid) (14), poly(malic acid) (14), polypeptides (14), poly(phospophazenes) (14), poly (ortho esters) (14), and chitosan (15). Anionic and nonionic surfactants are commonly used in DDS carriers (16), with these materials containing groups such as hydroxyl, oxyethylene, amine, phenyl, quarternary ammonium, and dialkyl phosphonate groups. Therefore typical chemical functional groups used in the drug delivery system carriers include hydroxyl, oxoethylene, phenyl, carboxylic acid, amine, dialkyl phosphonate, and esters. In previous studies (17,18), we studied the effect of oxyethylene and quaternary ammonium groups on the adhesion to a melanoma cell surface. We found that although all of these groups adhered to a cell surface, only the quaternary ammonium surface adsorbed strongly to the cell surface. However, as the surface of nonmalignant cells is negatively charged because of sialic acid residues of sugar-protein located in the cell membrane (19), these quaternary ammonium containing DDS carriers will also bind strongly to nonmalignant cells. In this way, these DDS carriers will not show specificity to a malignant cell, thereby failing the criteria of a functioning DDS. The effect of increasing the molecular weight of an oxyethylene adsorbed to a particle surface increased the adsorption of the modified particle, providing the oxyethylene chains did not contain entanglements or inter-chain hydrogen bonding (18). However, in order to obtain a binding adhesion between the particle and the cell surface that is strong enough, a long oxyethylene chain is generally required. The efficiency of the surfactants and polymers using oxyethylene groups as adhesion controlling groups is therefore low, due to the occurrence of entanglements or inter-chain hydrogen bonding with high molecular weight oxyethylene groups and the low adhesion obtained with low molecular weight oxyethylene groups. Instead of using quaternary ammonium or oxyethylene groups as the adhesion controlling groups in the DDS carriers, we may be able to use the hydroxyl, phenyl, carboxylic acid, amine, dialkyl phosphonate, and ester groups. Up to now the adhering ability of these groups has mostly only been investigated by using a polymer or surfactant that contains these and other chemical groups. The adhering ability of these individual groups to the surface of a melanoma cell and their comparison, however, does not appear to have been studied before.

In this study, we measured the ability of phenyl, carboxylic acid, amine, dialkyl phosphonate, ester, and hydroxyl groups to adhere to the surface of a living melanoma cell by using bare and modified silica or polystyrene particles. The magnitude of the adhesions were detected using the Atomic Force Microscope by attaching the particle to a cantilever and measuring the adhesion force between the particle and a living mouse skin melanoma cell (B16F10 cell) in a buffer solution. In this way we could directly determine which chemical groups could bind to a melanoma cell and which groups bound the strongest. In order to determine the specificity of these particles to the B16F10 cell, we then compared the strengths and variations in the adhesions of the particles, which bound the most and the least to the B16F10 cell, with those measured using a nonmalignant mouse cell (L929, mouse fibroblast cell). Such a direct and fundamental study does not appear to have been performed before. However, the results of this study give vital information, as to which surfactants or polymers should be used in the DDS carriers designed for malignant cells.

EXPERIMENTAL

Materials

Particles with a phenyl and a carboxylic acid containing surface were obtained by using a polystyrene particle (Mass mean average diameter $= 7.12 \pm 0.42 \mu m$, Bangs Laboratories, Fishers, IN, USA) and a carboxylic acid modified polystyrene particle (Mass mean average diameter $= 6.90 \pm 0.41 \mu m$, 114.7 $Å^2$/COOH surface group, Bangs Laboratories, Fishers, IN, USA). The hydroxyl surface was obtained by using bare silica particles (mass mean average diameter $= 6.84 \pm 0.57 \mu m$, Bangs Laboratories, Fishers, IN, USA). The silane coupling agents used to make an amine, dialkyl phosphonate, and ester modified particle surface were N-methylaminopropyltrimethoxysilane (Gelest, Morrisville, PA, USA), diethylphosphatoethyltriethoxysilane (Gelest, Morrisville, PA, USA), and acetoxypropyltrimethoxysilane (Gelest, Morrisville, PA, USA). The silicon wafers used to check the modification of the silane coupling agents were obtained from Shin-Etsu Co. Ltd. (Tokyo, Japan). The wafers were coated with a 2 nm natural oxide layer. The water used in this experiment was distilled and deionised to give a conductance of 18.2 MΩ cm^{-1} and a total organic content of 5 ppm.

Preparation of Probes

The way to modify silica particles using the silane coupling agents such as those described above and their surface characterisation were reported in another study (17,20). Briefly, the silica particles were modified with the silane coupling agents in the following way. 20 μl of the silica particles in water dispersion was added to 3 ml of an ethanol (99.5% EtOH, highest purity, Kishida Chemicals, Osaka, Japan.)-aqueous ammonia mixture (28 wt%, highest purity, Kishida Chemicals, Osaka, Japan.) (12.6EtOH: 1 NH_3) and was stirred for 2 h at 40°C. A solution consisting of 0.2 g of the silane coupling agent and 1 ml EtOH was then added drop-wise, and allowed to stir for a minimum of 18 h at 40°C. The particles were then washed a minimum of three times in solvent by centrifugation and decantation. The particles were subsequently dispersed in ethanol, and stored in a clean vessel.

The colloid probes of the above particles were prepared by evaporating the solvent from a small volume of the particles, and then attaching a single particle to a gold-plated $Si–Ni_4$ cantilever (spring constant=0.06 Nm^{-1}, NP–S, Veeco NanoProbe™ Tips, Nihon Veeco KK, Osaka, Japan), by using an XYZ micromanipulator and an epoxy resin (rapid araldite, Vantico, Showa polymer company, Tokyo, Japan).

Cell Cultivation and Cell Sample Preparation

The L929 (mouse fibroblast cell, Dainihonseiyaku) and B16F10 cell line (mouse skin cancer cells, obtained from the laboratory of Prof. Fukumori of Kobe Gakuin Univeristy, Kobe, Japan) were both cultured in the same way in a MEM medium (Eagle's MEM medium with kanamycin, without sodium bicarbonate, L-glutamine, Nissui Pharmaceutical, Tokyo, Japan), supplemented with L-glutamin (Nacalai Tesque, Kyoto, Japan) and Fetal bovine serum (FBS, JRH Biosciences, Lenexa, Kansas, USA). The medium was sterile filtered and sodium hydrogen carbonate (Nacalai Tesque, Kyoto, Japan) was used to adjust the pH to 7.4. The subculture of these cells was performed as follows. The culture flask (75 cm^2, No. 3110-075X, Iwaki, Tokyo, Japan) containing the cells to subculture was firstly washed with a buffer solution (Dulbecco's Phosphate-Buffered Saline without calcium chloride or magnesium chloride, PBS, Gibco, Invitrogen, Tokyo, Japan). Trypsin (Trypsin from Hog pancreas, Nacalai Tesque, Kyoto, Japan) was then used to remove the cells from the substrate, and a complete media solution (MEM solution containing FBS) was added, giving a cell concentration of 5×10^5 cell ml^{-1}. This cell suspension was filled 2 mm high in either a cell culture flask or a cell culture dish (40 mm diameter, No. 3000-035x, Iwaki, Tokyo, Japan); the flask allowed us to perform successive subcultures and the dish was used for the AFM experiments. The samples were stored in an incubator with an atmosphere of 5.0% CO_2 and a temperature of 37.0°C. These conditions ensured the pH of the complete media solution was 7.4.

The AFM culture dishes were kept in the incubator for 1 day after subculture, allowing a monolayer of cells to grow. The pH of the solution in the culture dish was maintained at 7.4 in the outside environment for several hours by removing the subculture complete media solution, washing with PBS, and then adding 1 ml L-15 (Leibovitz's L-15 Medium with L-glutamine, Gibco, Invitrogen, Tokyo, Japan). No FBS was contained in the L-15 solution, eliminating the effect of those polymers on the experimental results.

Instrumental: Atomic Force Microscope

The surface forces between a cell and colloid probe were measured in the L-15 solution as a function of their distance with an AFM (MFP-3D, Asylum Research, Santa Barbara, CA, USA). The transparent, cell culture dish was placed on the AFM stage (the *x*–*y* piezo), allowing the cells to be viewed by a light microscope, which was positioned below the AFM stage. The cantilever probe was fixed on the AFM head (the z-scanner) and positioned to face the cells.

A method based on the technique of Ducker and others (21) was used for the force measurements. Briefly, we determined the deflection change of the cantilever (Δx) as a function of the piezo displacement by monitoring the differential intensity of the reflection of the laser beam off the cantilever onto a split photodiode. Hooke's law, $F=k\Delta x$, was used to calculate the force (F), where k is the spring constant of the cantilever. The constant compliance region in the force curves was taken in the region just after the probe was in contact with the surface of a cell, where there was a linear relation between the measured separation distance and deflection distance (Δx) (22). In doing this, we presumed that the deflection of the cantilever was only due to the elastic deformation of the cell (23–25). Zero separation was subsequently characterized from the position of the onset of the linear compliance region in the force profile.

The force measurements were made by bringing the colloid probe in contact with the cell at a scan rate of 0.4 μms^{-1} (corresponding to a frequency of 0.05 Hz) and the minimum loading force needed to reach the cell surface and to give a compliance region. A comparison of the force curves obtained using higher scan rates showed that this frequency was low enough not to cause visco-elastic effects in the force curves. During this approach time the compression force data was collected. Once in contact, the probe was left on the cell surface for 5 min. We used this residence time, as we saw in an earlier study that the adhesions between a cell and a particle may increase with the time of contact between the probe and cell (26). A shorter residence time, e.g., 1 min, resulted in quite small adhesion forces, whereas a residence time of 5 min allowed us to obtain larger adhesion forces. Although the magnitude of the adhesion forces changed with time, the relative intensities of the adhesion forces of the different particle surfaces did not change with the residence time. Therefore this larger adhesion force allowed us to compare the adhesion differences between probe types more easily. Additionally, the approach of the colloid probe to the visco-elastic cell may have induced movement in the cell. Therefore, this residence time also ensured the cell surface was stationary before measuring the decompression force curves, thereby reducing or eliminating the risk of visco-elastic effects in the decompression force curves. After the residence time, the probe was moved away from the cell surface, while the data for the decompression force curve was collected. However, in the case of strong adhesions between the cell and the probe, the cell and probe did not always separate completely after the experiment. Additionally, the reasonably long residence time of the particle at the cell surface may cause the z-piezo to experience some drift. Thus, the probe was moved to another place after the measurement of a decompression force curve, and then immediately returned to its original position, in order to break any remaining bonds between the probe and cell. Another compression force curve was then collected, the baseline of which was used to define the zero force position for the decompression force curve.

The forces corresponding to each probe type were measured at the nucleus of at least 100 different cells. The forces were measured at the nucleus of the cell, as it was the highest position on the cell. Thus, the possibility of higher areas in the cell causing steric or other forces was then eliminated. The forces of only living cells were measured in this study, as the B16F10 and L929 cells lost their adhering ability to the substrate, when they died. A force study between a particle and a cell in a liquid medium requires the cells to adhere to the substrate.

Instrumental: Ellipsometry

As it was easier to characterize the surface of a silica substrate than a silica particle, we used ellipsometry to investigate the surface of silica wafers, which were modified

with the silane coupling agents in the same manner as the silica particles. The presence and thickness of an adsorbed film on a silica surface was determined using ellipsometry (M-2000U, J. A. Woolam, USA). The wavelength range used was 240–1,000 nm, and the angle of incidence was 70°. The thickness of the adsorbed films was estimated using the WVASE32 software, which enabled the raw data to be fitted with a layer model consisting of Si, SiO_2 and the adsorbed organic film. The values of the real and imaginary parts of the refractive index (n and k) and their variation as a function of wavelength were known for the Si and SiO_2 layers, and were used in the analysis. For a description of the organic film, a Cauchy model was applied with the refractive index of the corresponding silane coupling agents, which was informed by the supplier: n_D=1.413 and k=0 for the amine-modified, n_D=1.426 and k=0 for the dialkyl phosphonate-modified and n_D=1.415 and k=0 for the ester-modified films. Here, n_D denoted the refractive index at 589.3 nm.

RESULTS AND DISCUSSION

The adhesion strength between a living B16F10 cell and common chemical groups was investigated using particles with the surfaces drawn in Fig. 1. Particle surfaces with phenyl (*Phenyl*), carboxylic acid (*COOH*), and hydroxyl (*OH*) groups were obtained by using a bare polystyrene particle, a polystyrene particle functionalized with carboxylic acid, and a bare silica particle, respectively. Particles with amine (*NH*), dialkyl phosphonate (*Phos*), and ester (*Ester*) groups were obtained by modifying silica particles with N-methylaminopropyltrimethoxysilane, diethylphophatoethyltriethoxysilane, and acetoxypropyltrimethoxysilane, respectively, in the manner described in the experimental section. The adsorption of the silane coupling agents on silicon wafer surfaces were verified by ellipsometry, where measurement of the refractive index and dielectric constant of the modified surface in air allowed us to judge the presence of a monolayer. *NH*, *Phos*, and *Ester* modified surfaces gave adsorbed film thicknesses of 0.45±0.18, 0.42±0.19, and 0.36±0.04 nm, respectively. The modification of the silica particles, which gave uncharged surfaces, were subsequently verified by the absence of an electrostatic force, when the AFM was used to measure the force between the modified particles and a silica wafer in water. This is because the force between two unmodified silica surfaces in water (pH approximately 5.6) is reported to be a strong, long-range force (27), due to the nonnegligible charge on the silica surfaces under these conditions. The measured force curves also indicated that all the surface silanol groups had undergone a reaction with the silane coupling agents. Therefore, the number of surface functional groups in the *OH*, *NH*, *Phos*, and *Ester* particles could be thought to be the same. Additionally, as the size of the polystyrene and silica particles were approximately the same and as the separation distance between neighboring phenyl groups and neighboring silanol groups on the polystyrene and silica particles, respectively, are similar, the number of functional groups on the *Phenyl* and *OH* particles could be thought to be comparable. Finally, comparison of the forces measured for the *Phenyl* and *COOH* particles with the cells gave the effect of the carboxylic acid groups on the binding, as the COOH particle was a carboxylic acid modified polystyrene particle. Therefore, the forces measured between the cells and the particles with the *Phenyl*, *COOH*, *NH*, *Phos*, *Ester*, and *OH* surfaces were directly compared in this study.

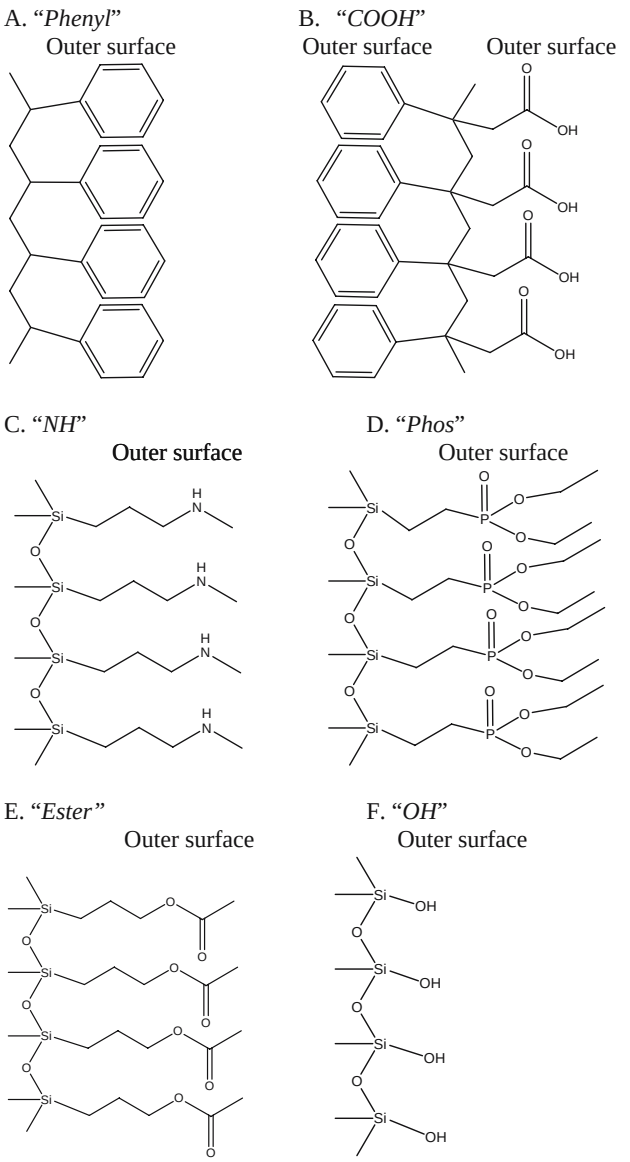

Fig. 1. Surface groups of particles used in this study. **A**–**F** show the imaged outer surface of a "*Phenyl*", "*COOH*", "*NH*", "*Phos*", "*Ester*", and "*OH*" particle, respectively.

The interaction between the particles and the living B16F10 cells were observed by using the AFM to measure the force between a particle, which was attached to a cantilever, and a living cell. As the cells were living and therefore displayed differences in their surface properties, a minimum of 100 force curves were collected, using 100 different cells. Examples of a force curve obtained for *Phenyl*, *COOH*, *NH*, *Phos*, *Ester*, and *OH* are shown in Fig. 2A–F, respectively, where the compression and decompression force curves are given by the solid grey circles and the open black circles, respectively. For each particle type, the compression curve displayed no attractive or repulsive force at long or medium particle-cell separations, until a

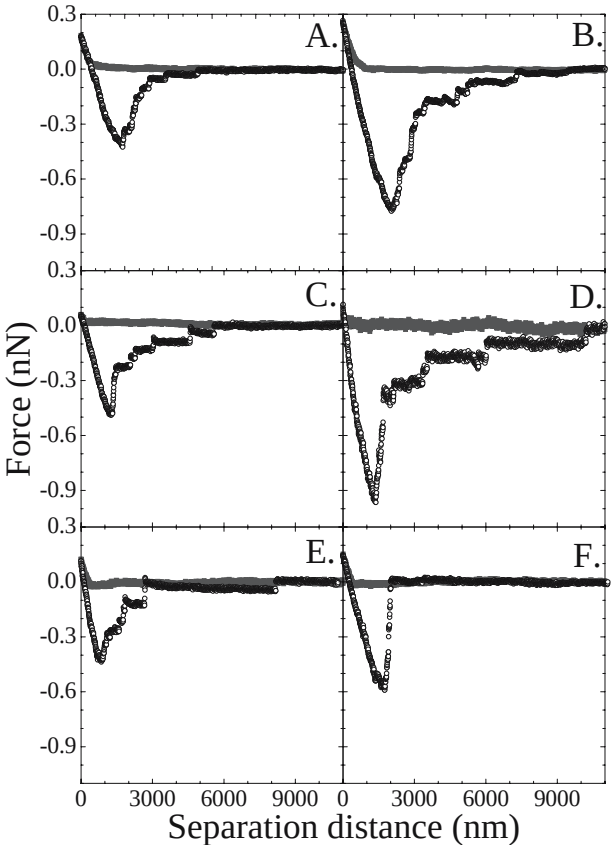

Fig. 2. Typical force curves measured between the various particles and a living B16F10 cell in L-15. **A** *Phenyl* particle force curves; **B** *COOH* particle force curves; **C** *NH* modified particle force curves; **D** *Phos* modified particle force curves; **E** *Ester* modified particle force curves; **F** *OH* particle force curves.

repulsive force was detected at small separations. As we measured the forces in L-15, a buffer solution with a high ionic strength, we could think that this repulsive force was not electrostatic in origin. Instead, this force was probably a steric or visco-elastic force, the latter resulting from the visco-elastic property of a cell (28). The lack of an attraction suggested that these particles did not immediately enter the B16F10 cell. Additionally, the lack of a longer ranged repulsive force suggested that the particles with these surface types were not being immediately rejected by the B16F10 cells. During the residence time, no change in the force between the cell and the particle was detected, and the particle was not seen to enter the cell. These facts suggested that endocytosis of the particle was not occurring during this time period, and that the attraction in the decompression force curve was most likely due to the breaking of the bonds between the cell and the particle. The decompression force curves for each of these surface types showed an attraction, indicating the presence of an adhesion between the cell and each particle. The maximum of this adhesion (F_{admax}) has been suggested to indicate the strength of the adhesion between a cell and a particle (29,30), where a larger F_{admax} would indicate a stronger adhesion. It is at this point, where the majority of bonds between the particle and cell were thought to be broken. For each surface type, one main adhesion peak was observed, suggesting that the adhesions were due to bonds between the cell and particle that were in parallel (31). Several smaller adhesions at larger particle-cell separations were observed for each surface type. These may be the result of stronger bonds being broken, as a stronger bond would require a larger energy or a larger separation distance in order to be broken (31). Alternatively, the smaller peaks may be tether points, due to the breaking of ligand-receptor or nonspecific bonds. These bonds may have reformed after being broken at F_{admax}, as the cell and particle had not completely separated at this separation distance. Such a behavior has been noted by Leckband and Israelachvili (31). The complete breaking of the bonds between the cells and particles, however, required several thousand nm. This may also suggest the progressive detachment of the adhesive contacts.

The forces measured by the AFM gave the total force between the particle and the cell surface in the L-15 solution. This means that we could not directly discern the origin of the forces, as an attraction may have been due to electrostatic, chemical, van der Waals or hydrogen bonding origins. We could, however, deduce possible origins by firstly considering the types of materials in our systems and the forces available for such systems, and then by comparing the measured forces with the expected profiles of the plausible forces in our systems. Although this method is relatively simple in a system with somewhat well-defined surfaces, it is more difficult in a cancerous cell system, whose surface properties are still much unknown. Therefore, in order to deduce the origin of the adhesions between the particles and the cells, we needed to compare the forces for several types of particle-L15 solution–cell systems and to consider their possible forces.

Possible physical forces acting between the particles and the cells include the electrostatic (repulsive or attraction), van der Waals (attractive), and hydrogen bonding (attractive) forces. As no long-ranged attractive force was detected between any of our particle types when their force was measured against a negatively charged substrate in water, we could conclude that the quantity of positive charges on our particles was low or negligible. Additionally, as the ionic strength of the L-15 solution is high (>140 mM), we could expect a negligible or minimal contribution of the electrostatic repulsion in our system, even if the particle surfaces contained charges. This is because the magnitude of the repulsive electrostatic force decreases with the ionic strength of the solution. The strength of the van der Waals force is dependant on the Hamaker constant of the system, whose value can be calculated using a combining relation the Hamaker constant of each surface and the medium in vacuum (32). As L-15 and the cell surfaces are used in each system, the only variable can be thought to be the particle surface. However, the Hamaker constant of polystyrene and fused quartz (a material with properties similar to silica) across vacuum are 6.6×10^{-20} and 6.5×10^{-20} J, respectively (33). As these two surfaces are imagined to be the two most different particle surface types in our study and as their Hamaker constant values are similar, we can expect to see little difference in the magnitude of the van der Waals force for each particle type used in this study. In addition to the van der Waals force, the *Phenyl* group may be expected to also bind via hydrophobic forces, due to its hydrophobicity.

Additionally, as the *OH*, *COOH*, *NH*, *Phos*, and *Ester* surfaces contained groups that could participate in hydrogen-bonding, hydrogen bonds between these particle surfaces and the cells may also give adhesions. The effect of the hydrogen bonding strength may be obtained by comparing the magnitudes of the adhesion between the *Phenyl* and the other surface types, as only the *Phenyl* is expected not to undergo hydrogen bonding.

Possible chemical reactions that may have occurred between the particles and the functional groups on the cell surface include a reaction between: 1., the hydroxyl group of *OH* with the hydroxyl groups on the cell surface to give an ether (34), where hydroxyl groups can be found in amino acids, the polar head-groups of a membrane phospholipids, and sugar residues (35); 2., a phenyl group on *Phenyl* and an acyl group on the cell surface (36), e.g., an acyl group found in amino acid and sugar residues (35); 3., the carboxyl acid groups of *COOH* with the hydroxyl groups on the cell surface to give an ester (37); 4., the reaction of the secondary amine group in *NH* with aldehyde or ketone groups on the cell surface to give a tertiary amine (38), where ketone groups can be found in the Asparagine and Glutamine amino acids, membrane lipids, and sugar residues (35); 5., the reaction of *Phos* with an amine (39), a carbonyl (40) or an imine group (40), where amine groups can be found in amino acids (35), phospholipids (35), and sugar residues (35), carbonyl groups can be found in amino acids (35) and sugar residues (35), and imine groups can be found in amino acids (35); and 6., the reaction of an ester group on *Ester* with hydroxyl groups or amine group on the cell surface to give a different ester (41) or an amide (41), respectively, where amine groups may be found in the amino acids and membrane phospholipids on a cell surface (35).

More information on the origin of the bonds seen in our system may be obtained, if we compare the magnitude of F_{admax} of each surface type. If all surface types display approximately the same F_{admax}, which is greater than zero, then we can conclude that van der Waals is the main binding mechanism. If the F_{admax} for *OH*, *COOH*, *NH*, *Phos*, and *Ester* is approximately the same, but is greater than *Phenyl*, which is non-zero, then we can conclude that the binding mechanisms for *OH*, *COOH*, *NH*, *Phos*, and *Ester* occurred via an attractive van der Waals force and hydrogen bonding. If the F_{admax} values for some of *Phenyl*, *OH*, *COOH*, *NH, Phos*, and *Ester* are greater than the F_{admax} of the other surfaces, then we can assume the additional presence of additional bonding, such as chemical bonding.

We can directly compare the binding, i.e., F_{admax}, of each surface type to the B16F10 cell, as each particle had approximately the same size and as we used the same residence times of the particles at the surface of the cells. These conditions were seen from previous studies (26), which showed that the adhesion between a cell and a particle may increase with the adhesion time and with the particle size. As the F_{admax} varied between the 100 different B16F10 cells used for each surface type, we obtained the average F_{admax} ($<F_{admax}>$) by making a histogram of the F_{admax} measurements for each particle type, and fitting a Lorentzian curve to the histogram. The peak of the Lorentzian curve gave $<F_{admax}>$. The standard deviation (*std*) of the F_{admax} was calculated using the $<F_{admax}>$ determined from the Lorentzian fitting and the F_{admax} data. The magnitude of $<F_{admax}>$ indicates the adhesion strength of the functionality type to the cell surface. The *std* can be thought to depict the variation in the surface properties of cells, i.e., the differences in the number of groups on the cell surface that can bind with the particle for the individual cells. As cancerous cells are reported to show large deviations in the number of functional groups on their surfaces, e.g., the number of integrins and glycoproteins (43–47), a large *std* can be expected for cancerous cells.

The histograms of *Phenyl*, *COOH*, *NH*, *Phos*, *Ester*, and *OH* are given in Fig. 3A–F, respectively. A summary of the $<F_{admax}>$, shown by the black bar graph, and its *std*, shown by the open bar graphs with diagonal lines, are given in Fig. 4 for each surface type. We can see that the order of $<F_{admax}>$ for the different surfaces is: *Phenyl*<*Ester*<*OH*, *NH*, *Phos*<*COOH*. As the *COOH* surface is a carboxylic acid functionalized polystyrene particle, this surface can be thought of consisting of both *COOH* and phenyl groups. However, even if we subtract the $<F_{admax}>$ of a nonfunctionalized polystyrene particle, *i.e.*, *Phenyl*, we can see that the *COOH* particle still gives the strongest $<F_{admax}>$. The low $<F_{admax}>$ value of *Phenyl* suggests only weak binding via van der Waals forces to the cells by the particles. The higher $<F_{admax}>$ values of *Ester*, *OH*, *NH*, *Phos*, and *COOH* suggest additional means of binding. As *Ester*, *OH*, *NH*, *Phos*, and *COOH* are all capable of hydrogen bonding, this may contribute to the

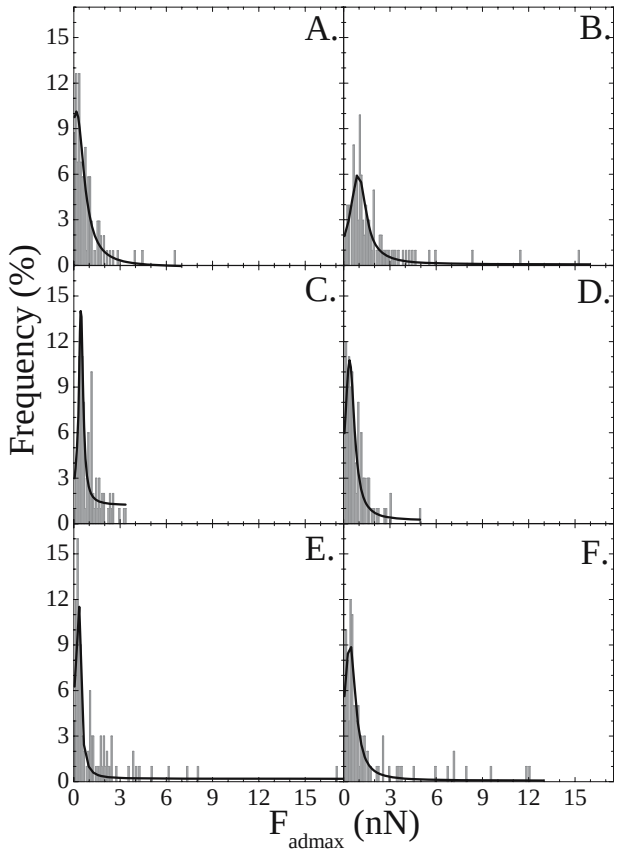

Fig. 3. The histogram of the F_{admax} obtained with the living B16F10 cells in L-15 from **A** 103 *Phenyl* force curves; **B** 101 *COOH* force curves; **C** 100 *NH* force curves; **D** 100 *Phos* force curves; **E** 100 *Ester* force curves; and **V** 103 *OH* force curves. The *solid line* shows the Lorentzian fitting to the percentage of F_{admax} *vs* F_{admax} histograms.

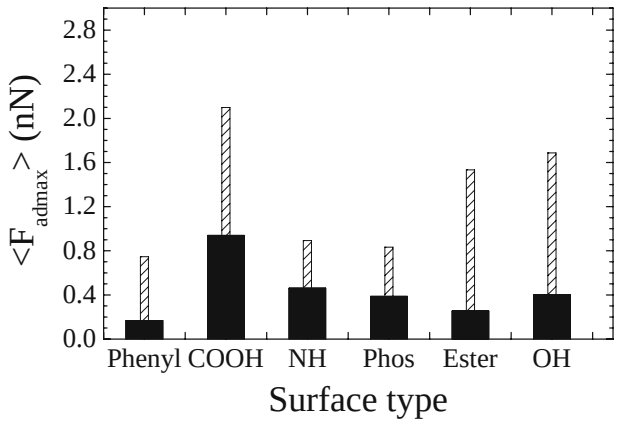

Fig. 4. Summary of $<F_{admax}>$ and *std* for the interaction of a particle and a living B16F10 cell as a function of the different surface types. The $<F_{admax}>$ was obtained from the Lorentzian fitting of the F_{admax} histograms (*solid large bars*) and *std* (*thin bars*) calculated using the $<F_{admax}>$ values and the F_{admax} data.

stronger binding. The difference in the adhesion magnitudes of *Ester*, *OH*, *NH*, *Phos*, and *COOH* may lie in the difference in the strength and reaction rates of the possible chemical bonding between the different particle types and the cells. We can obtain some further indication as to the bond origins, if we additionally look at the variation in the *std* values in the $<F_{admax}>$ data shown in Fig. 4 for all the particle types. Here, we see that *Ester*, *OH*, and *COOH* all have high *std* values, while *NH*, *Phos* and *Phenyl* have a lower value. The low $<F_{admax}>$ and *std* values of *Phos* suggest that this particle is not binding via chemical bonding, but rather is probably binding via a van der Waals and hydrogen bonding. The lower $<F_{admax}>$ and *std* values for *NH* suggest little chemical binding is occurring for this group. The larger value of $<F_{admax}>$ for *NH* compared to *Phos* may, however, be explained in terms of a weak electrostatic attraction occurring between the *NH* groups and the negatively charged mucus network or glycocalyx on the cell surface (42). This is possible, as the *NH* groups may be slightly protonated in the L-15 solution. The much lower adhesion value of *NH* compared to the large adhesion seen by a quarternary ammonium group to a B16F10 cell (17) can be explained by a low degree of prototation of the *NH* group, as suggested by the lack of a strong adhesion being observed between the *NH* particle and a negatively charged mica surface in water. As the chemical reaction between *Phenyl* and an acyl group generally requires the high temperatures (80°C) not applicable for cells, the *Phenyl* group can be thought to bind to the cell surface via van der Waals forces and hydrophobic bonding with hydrophobic portions on the cell surface, e.g., the nonpolar amino acids (35). The high *std* values for *Ester*, *OH*, and *COOH* suggest that these groups may be chemical binding to groups that are overexpressed on the cancer surface, in addition to binding via van der Waals and hydrogen bonding. The B16F10 cell is reported to over-express certain integrins and glycoproteins, such as alpha-4 beta-1 integrin (43), Interleukin-2 (44), the CD44 receptor (45,46), and Dok 1 (47). As many of these structures contain hydroxyl groups, the *Ester*, *OH*, and *COOH* groups may be reacting with the hydroxyl group of the over-expressed integrins and glycoproteins, forming a bond between the particle and the cell. However, the lower $<F_{admax}>$ values of *Ester* and *OH* suggest that the chemical reactions with hydroxyl groups are less likely to occur than that for the *COOH*. The reaction between an ester and alcohol group require both heat and an acidic environment (41), and a reaction between two alcohol groups require heat. The reaction between a carboxylic acid and a hydroxyl group is reported to occur only very slowly in the absence of strong acids and requires several hours to reach equilibrium in such an environment (48). The fact that we observed significant binding between *COOH* and the cells within a 5 min residence time of the functionalized particle at the cell surface in the presence of the neural L-15 medium suggested that there may have been acidic areas on the cell surface that catalyzed this reaction.

Although it has been reported for polymer systems that electronegative charges reduce their uptake by tumor cells by repulsion (49), the adhesion of COOH to the cells can be explained by the fact that the electrostatic repulsive force is weak/negligible in our system due to the high ionic strength of L-15, and that the magnitude of the covalent bonding is strong and nonnegligible. The magnitude of the covalent energy between a 6.84 μm diameter sized modified silica particle and a surface containing bondable groups may approximated as being between $2.7\times10^{-6}$and 1.1×10^{-2} mNm^{-1}, if one or all functional groups, respectively, bind (see Appendix 1 for the calculation). The maximum energy calculated from experimental results of a system containing van der Waals and electrostatic force possibilities in a L-15 solution is only 2.4×10^{-2} mNm^{-1} (see Appendix 2 for the calculation). As more than one chemical bond is likely to occur in our system, we can conclude that the attractive force should be stronger than the electrostatic force. This probably allows thereby our particles to adhere to the cell.

In order to determine the specificity of these particles to the cancerous B16F10 cell (mouse skin melanoma cell), we used the particle that showed a high $<F_{admax}>$ and a high *std* to the B16F10 cell, i.e., *COOH*, and the particle with the lowest $<F_{admax}>$ and a lower *std* to the B16F10 cell, i.e., *Phenyl*, to measure their adhesion strengths to the noncancerous L929cell (mouse fibroblast cell). Although it is best to use mouse skin non-melanoma cells for comparison with B16F10 cells, we chose to use the non cancerous mouse fibroblast cell due to their ease of cultivation. The interaction between the particles and the living L929 cells were again observed using the AFM , where a minimum of 100 force curves were collected for each particle type. Examples of a force curve obtained for *Phenyl* and *COOH* are shown in Fig. 5A and B, respectively, where the compression and decompression force curves are given by the solid grey circles and the open black circles, respectively. In both cases, the compression curve displayed no attractive or repulsive force at long or medium particle-cell separations. A repulsive force was detected at small separations, again presumably a steric or visco-elastic force. Both particle types are thought not to undergo endocytosis with the L929 cell, because of an absence of an attraction in the compression force curves and because the force between the cell and the particle was not seen to change during the residence time. The decompression force curves displayed an attraction, indicating the

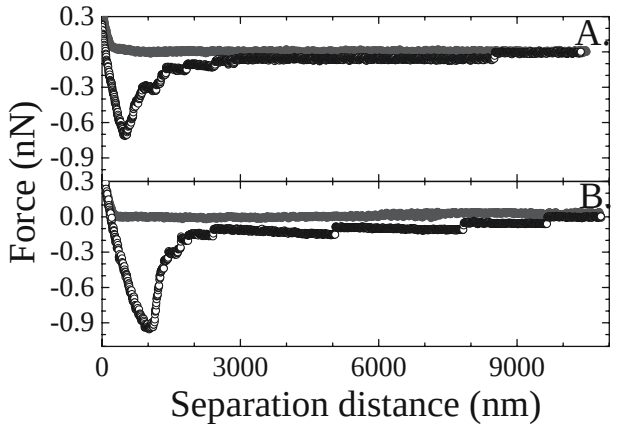

Fig. 5. Typical force curves measured between the various particles and a living L929 cell in L-15. **A** *Phenyl* particle force curves; **B** *COOH* particle force curves.

presence of an adhesion between the cell and each particle. The maximum of this adhesion again presumably indicates the strength of the adhesion between a cell and a particle (29,30).

Figure 6 shows the F_{admax} histogram for the *Phenyl* surface–L929 cell interaction as solid dark grey bars and the Lorentzian fitting as a solid line. The F_{admax} histogram for the *Phenyl* surface–B16F10 cells (open bars) and its Lorentzian fitting (dotted line) is also shown in Fig. 6 for comparison. Figure 7 shows the F_{admax} histograms for the *COOH* surface–L929 cell interaction (solid grey bars) and its Lorentzian fitting (solid line), and the F_{admax} histogram for the *COOH* surface–B16F10 cells (open bars) and its Lorentzian fitting (dotted line) for comparison. The $<F_{admax}>$ and *std* for the *Phenyl* and *COOH* surfaces for both the B16F10 and L929 cells are additionally summarized in Fig. 8. Here, the black solid bars and the grey bars with horizontal lines indicate the $<F_{admax}>$ data for the B16F10 and L929 cells, respectively, and the open bars with diagonal lines display the *std* of the F_{admax} data. We can firstly see from these figures that the spread of the F_{admax} data, i.e., *std*, is significantly reduced for both the *Phenyl* and *COOH* particles in the case of the L929 cell, when compared to the data for the B16F10 cell. This indicates that there is much less variation in the surface

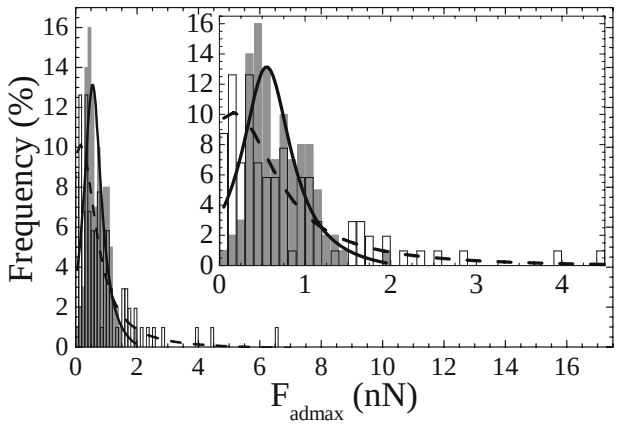

Fig. 6. The histogram of the F_{admax} obtained from *Phenyl* showing the F_{admax} determined from 100 force L929 cells (*solid grey bars*) and its Lorentzian fitting (*solid line*), and the F_{admax} determined from 103 force B16F10 cells (*open bars*) and its Lorentzian fitting (*dotted line*).

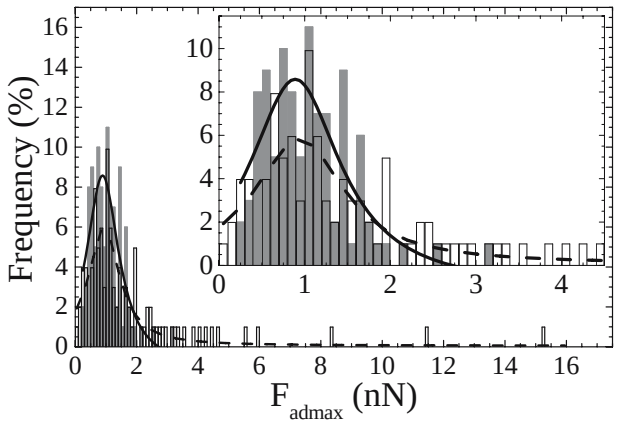

Fig. 7. The histogram of the F_{admax} obtained from *COOH* showing the F_{admax} determined from 100 force L929 cells (*solid grey bars*) and its Lorentzian fitting (*solid line*), and the F_{admax} determined from 101 force B16F10 cells (*open bars*) and its Lorentzian fitting (*dotted line*).

properties of the noncancerous cells, when compared to the variation in the cancerous cells. Secondly, we can see that the $<F_{admax}>$ of *Phenyl* was lower for the B16F10 cell than that for the L929 cell. As the strength of the van der Waals bonding of the *Phenyl* surface with the cell surface is unlikely to vary significantly, this significant increase in its bonding to the L929 cells suggests that the strength of the hydrophobic bonding of the particle with cell surface was increasing. A decrease in the number of hydrophilic groups on the cell surface may cause such a phenomenon. Finally, the *COOH* group can be seen to show a lower $<F_{admax}>$ for L929 when compared to that for the B16F10 cells. Additionally, the *COOH* histograms of Fig. 7 show that many B16F10 cells bound to the *COOH* particle with strengths much greater than the $<F_{admax}>$ and had F_{admax} values outside of the Lorentzian fitting region shown for the noncancerous cells. These data suggest that the number of sites on the L929 cell that may bind to the *COOH* surface is less than on the B16F10 cell. This may be a result in the lower number of

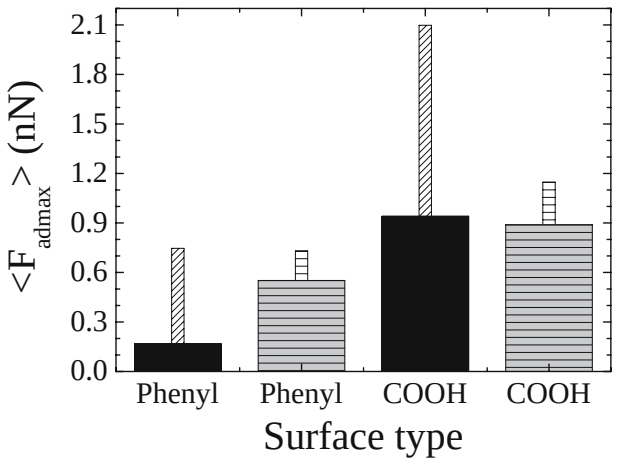

Fig. 8. Summary of $<F_{admax}>$ and the *std* for the interaction of the *Phenyl* and *COOH* particles with living *B16F10* and *L929* cells. The thick *solid black bars*, $<F_{admax}>$ for B16F10 cells; *thick grey bars with horizontal stripes*, $<F_{admax}>$ for the L929 cells; *thin bars with diagonal stripes*, the *std* for the B16F10 cells; *thin bars with horizontal stripes*, the *std* for the L929 cells.

hydroxyl containing groups on the L929 cell, compared to the B16F10 cell, which is reported to overexpress the integrins and glycoproteins (hydroxyl containing groups).

ADDITIONAL REMARKS

The above data shows that the *COOH* functionalised surface bound the strongest to the living B16F10 cells under our experimental conditions. However, in order to deem the applicability of this data to other situations, e.g., different residence times and systems, we should also consider the following points.

The above data was obtained using a residence time of 5 min for the particle at the living cell surface. A shorter residence time, e.g., 1 min, resulted in quite small adhesion forces, whereas a residence time of 5 min allowed us to obtain larger adhesion forces. Although the magnitude of the adhesion forces changed with time, the relative intensities of the adhesion forces of the different particle surfaces did not change with the residence time. Similarly, the size of the particle is not expected to affect the relative magnitudes of the adhesion strengths of the particles to the cells. However, the magnitude of the adhesion is expected to increase and decrease for larger and smaller sized particles. This is because the adhesion magnitude is related to the number of bonds between the surfaces, where a larger bond number would give a stronger force. However, as endocytosis is expected to occur for the particles whose surface is completely involved with strong binding events with the cells, a smaller particle will most likely under endocytosis easier than a larger particle. In our study, we chose to use the 6.84 μm sized particle, as its size is large enough to allow its attachment to a cantilever probe. As is also much smaller than the size of a nucleus of a B16F10 cell, it is also small enough to investigate the adhesion to the surface of cell nucleus.

Our Leibovitz's L-15 medium used in the AFM force measurements contained a wide variety of amino acids, which may also have bound to our probes. However, we believe that the presence of these amino acids did not greatly influence the relative adhesion intensities of the different probe functionality types to the living cells. This is because of the following reasons. The presence of a bond between the probes and the living cells showed that not all the binding sites on the probe had been occupied by the L-15 amino acids, or that the binding strength between the L-15 amino acids and the functionalized probes was weaker than the binding strength between the probes and groups on the living cell. The absence of a bond between the probes and the cells would have suggested that all of the binding sites on the probes had been occupied by the L-15 amino acids. Additionally, although each of the functionality types had the potential of binding with amino acids, we still saw a dependence of the binding strength of the probe type with the living cells. This showed that the binding of the probes to the cell surface was not being overly influenced by the L-15 solution.

The B16F10 and L929 cells used in the force measurements were presumably in different cycle stages, as it was not possible to adjust the cell cycle of the B16F10 and L929 cells to be identical for the AFM measurements. The number and type of functional groups on the cell surfaces may be dependant on the cell cycle. We therefore needed to minimize the influence of this effect on the relative probe functionality binding strengths to the cell surface by taking force curves of many different cells. We believe that data taken from 100 different cells minimized this effect, as we were able to see a distinct difference in the binding strength of the different probe types to the B16F10 and L929 cells.

In our study, we used particles whose surfaces were either bare or completely modified. This choice of system therefore did not allow us to study the effect of the surface functional group density or the subject of multivalency on the binding magnitude of the particles to the cells. Although peptide targeting moieties show that multivalency significantly enhances binding affinity (50), we chose to use our systems in order to ascertain the relative binding strength of each functional group. A partially modified particle would give a particle with various numbers and types of surface functionality groups. The forces of such systems are much more difficult to interpret, making it hard to ascertain the factors affecting the adhesion magnitudes to cells. As we now understand the qualitative strength of each functional group, a future study may be to vary the densities of functional groups. This would allow us to not clarify whether a variation in the density of functional groups on the surface can overcome the relative binding effects seen in this study.

As a result of these facts and the data of our study, we therefore believe that a carboxylic acid group is targeting a malignant cell. Thus, it appears useful to use carboxylic acid groups in a DDS carrier targeted for malignant cells.

CONCLUSIONS

We studied the adhesion of common chemical groups to living B16F10 cells by using particles containing a hydroxyl, phenyl, carboxylic acid, amine, dialkyl phosphonate, and ester groups. The hydroxyl, phenyl, and carboxylic acid surfaces were obtained by using a bare silica particle, a bare polystyrene, and a carboxylic acid modified polystyrene particle, respectively. The amine, dialkyl phosphonate, and ester surface was obtained by using silica particles and the appropriate silane coupling agent.

The magnitude of the average adhesion force measured between 100 cells and the particles indicates the adhesion strength of the particle surface to the cells. The standard deviation in the adhesion force strength data showed the variation in the cell surface properties for the 100 different cells. The carboxylic acid group showed the highest adhesion and a large standard deviation, when its force was measured against a B16F10 cell. The phenyl group gave the lowest adhesion and a lower standard deviation, when its force was measured against a B16F10 cell. Therefore, the phenyl group was thought to bind via a van der Waals and hydrophobic force attraction. The carboxylic acid group was thought to bind via a van der Waals attraction, hydrogen bonding, and significant chemical binding, due to reactions between the carboxylic acid and the integrins or glycoproteins overexpressed on the cell surface, which contained hydroxyl groups.

The comparison of the standard deviations of the forces measured between the phenyl and carboxylic acid modified particle surfaces and a noncancerous cell (L929) with the

data obtained for the cancerous B16F10 cell showed a considerably lower standard deviation in the force adhesion maximum for the L929 cells compared to the B16F10 cells. This fact suggested that the there is much less variation in the surface properties of the noncancerous cells, when compared to the variation in the cancerous cells. The adhesion maximum of the phenyl and carboxylic acid groups increased and decreased, respectively, for the L929 cells. A decrease in the number of hydroxyl containing groups on the cell surface for the noncancerous cell would cause an increase in the hydrophobicity of the cell surface, allowing a greater hydrophobic bonding ability between the L929 cell and the phenyl surface. A lower number of hydroxyl containing groups would simultaneously decrease the chemical bonding ability between the carboxylic acid groups and the L929 cells.

As the carboxylic acid group bound the strongest to the cell, it was thought the best to use in DDS systems formulated to target malignant cells.

ACKNOWLEDGEMENTS

Cathy McNamee would like to thank the Japanese Government for the financial support provided through the JSPS Postdoctorial Fellowship For Foreign Researchers.

APPENDIX 1.

Approximation of strength of cohesive force between modified silica particles and another surface containing bondable functional groups

The strength of the chemical bonding in the system (E_{chemall}) can be approximated as

$$E_{\text{chemall}} = N_{\text{bind}} E_{\text{chem1}} \tag{A1.1}$$

Where E_{chem1} is the strength of a single chemical bond, and N_{bind} is the number of binding sites on the particle.

N_{bind} can be determined by calculating the surface charge density (σ) on the particle and the surface area of the particle:

$$N_{\text{bind}} = \frac{\sigma 4\pi R^2}{e} \tag{A1.2}$$

Where R and e are the radius of the particle and the electronic charge.

The value of σ may be approximated using (51)

$$\sigma = (8C_{ei}\varepsilon_r\varepsilon_0 k_B T)^{1/2} \sinh\left(\frac{e\Psi_0}{2k_B T}\right) \tag{A1.3}$$

Where C_{ei} is the concentration of the ions in the bulk solution, and ε_r, ε_0, k_B, T, and ψ_0 are relative permittivity of the solution, the permittivity of vacuum, the Boltzmann constant, the absolute temperature, and the surface potential on the particle, respectively. As we modified the silica particles in neutral solution, we choose to approximate the system by using the ψ_0 of a silica particle (−60 mV) measured at pH 7 in 1 mM $NaNO_3$, as reported by Hartly and others (27).

As the strength of E_{chem1} is reported to between 100 kBT and 800 kBT (52), the value of N_{bind} for our system can be approximated as being between 2.7×10^{-6} and 1.1×10^{-2} mNm^{-1}, depending on whether one or all functional groups bind.

APPENDIX 2.

Determination of the maximum force measured in a nagetively charged particle-L-15 solution—negatively charged substrate system.

The F/R plot of a silica–L-15 solution-mica system showed a maximum force of 1.5 mNm-1 (26). Although this system used a 3.1 μm diameter particle, we may convert this value to an energy of our system (silica particle diameter 6.84μm) by using the Derjaguin approximation (53),

$$E = \frac{F}{2\pi R} \tag{A2.1}$$

Where E is the energy of the system, F is the measured force, and R is the radius of the particle. Here, we calculate the E as 2.4×10^{-1} mNm^{-1}.

REFERENCES

1. S. Neidle and D. E. Thurston. Chemical approaches to the discovery and development of cancer therapies. *Nat. Rev. Cancer.* **5**:285–296 (2005).
2. Y. Fukumori and H. Ichikawa. Nanoparticles for cancer therapy and diagnosis. *Adv. Powder Technol.* **17**:1–28 (2006).
3. P. Caliceti and F. M. Veronese. Pharmacokinetic and biodistribution properties of poly(ethylene glycol)-protein conjugates. *Adv. Drug Deliv. Rev.* **55**:1261–1277 (2003).
4. A. P. Chapman. PEGylated antibodies and antibody fragments for improved therapy: a review. *Adv. Drug Deliv. Rev.* **54**:531–545 (2002).
5. M. Ferrari. Cancer nanotechnology: opportunities and challenges. *Nat. Rev. Cancer.* **5**:161–171 (2005).
6. K. Petrak. Essential properties of drug-targeting delivery systems. *Drug Discov. Today* **10**:1667–1673 (2005).
7. C. C. Muller-Goymann. Physicochemical characterization of colloidal drug delivery systems such as reverse micelles, vesicles, liquid crystals and nanoparticles for topical administration. *Eur. J. Pharm. Biopharm.* **58**:343–356 (2004).
8. C. J. Drummond and C. Fong. Surfactant self-assembly objects as novel drug delivery vehicles. *Curr. Opin. Colloid Interface Sci.* **4**:449–456 (1999).
9. M. J. Lawrence and G. D. Rees. Microemulsion-based media as novel drug delivery systems. *Adv. Drug Deliv. Rev.* **45**:89–121 (2000).
10. D. D. Lasic and D. Needham. The "Stealth" Liposome: a prototypical biomaterial. *Chem. Rev.* **95**:2601–2628 (1995).
11. A. N. Lukyanov, T. A. Elbayoumi, A. R. Chakilam, and V. P. Torchilin. Tumor-targeted liposomes: doxurubin-loaded long-circulating liposomes modified with anti-cancer antibody. *J. Control. Release* **100**:135–144 (2004).
12. W. Maison and J. V. Frangioni. Improved chemical strategies for the targeted therapy of cancer. *Angew. Chem. —Int. Edit.* **42**:4726–4728 (2003).
13. G. Kaul and M. Amiji. Long-circulating poly(ethylene glycol)-modified gelatin nanoparticles for intracellular delivery. *Pharm. Res.* **19**:1061–1067 (2002).
14. M. Malmsten. *Surfactants and Polymers in Drug Delivery*. Marcel Dekker, Inc., New York, 2002, p. 294.
15. L. F. Qi and Z. R. Xu. *In Vivo* antitumor activity of chitosan nanoparticles. *Bioorg. Med. Chem. Lett.* **16**:4243–4245 (2006).
16. M. Malmsten. *Surfactants and Polymers in Drug Delivery*. Marcel Dekker, Inc., New York, 2002, p. 7.

17. C. E. McNamee, N. Pyo, and K. Higashitani. Atomic Force Microscopy study of the specific adhesion between a colloid particle and a living melanoma cell: effect of the charge and the hydrophobicity of the particle surface. *Biophys. J.* **91**:1960–1969 (2006).
18. C. E. McNamee, S. Yamamoto, and K. Higashitani. Joint effect of the chemical and physical properties of poly(ethylene gycol) brushes on their binding ability to living melanoma cells. *Biophys J.* **93**:324–334 (2007).
19. A. Alberts, A. Johnson, J. Lewis, M. Raff, K. Roberts, and P. Walter P. (eds.). *Molecular biology of the cell*, Garland Science, New York, 2002, p. 592.
20. K. Ohno, T. Morinaga, K. Koh, Y. Tsujii, and T. Fukuda. Synthesis of monodisperse silica particles coated with well-defined, high-density polymer brushes by surface-initiated atom transfer radical polymerization. *Macromolecules* **38**:2137–2142 (2005).
21. W. A. Ducker, T. J. Senden, and R. M. Pashley. Direct measurement of colloidal forces using an atomic force microscope. *Nature* **353**:239–241 (1991).
22. S. B. Velegol and B. E. Logan. Contributions of bacterial surface polymers, elastrostactics, and cell elasticity to the shape of AFM force curves. *Langmuir* **18**:5256–5262 (2002).
23. A. Razatos, Y. L. Ong, M. M. Sharma, and G. Georgiou. Molecular determinants of bacterial adhesion monitored by atomic force microscopy. *Proc. Natl. Acad. Sci. U.S.A.* **95**:11059–11064 (1998).
24. T. A. Camesano and B. E. Logan. Probing bacterial electrosteric interactions using atomic force microscopy. *Environ. Sci. Technol.* **34**:3354–3362 (2000).
25. Y. L. Ong, A. Razatos, G. Geogiou, and M. M. Sharma. Adhesion forces between E-coli bacteria and biomaterial surfaces. *Langmuir* **15**:2719–2725 (1999).
26. C. E. McNamee, N. Pyo, S. Tanaka, I. U. Vakarelski, Y. Kanda, and K. Higashitani. Parameters affecting the adhesion strength between a living cell and a colloid probe when measured by the atomic force microscope. *Colloid Surf. B-Biointerfaces* **48**:176–182 (2006).
27. P. G. Hartley, I. Larson, and P. J. Scales. Electrokinetic and Direct Force Measurements between Silica and Mica Surfaces in Dilute Electrolyte Solutions. *Langmuir* **13**:2207–2214 (1997).
28. M. Radmacher. Measuring the elastic properties of living cells by the atomic force microscope. In B. P. Jena and J. K. H. Hörber (eds.), *Methods in Cell Biology*, Academic, Amsterdam, 2002, p. 67.
29. O. H. Willemsen, M. M. E. Snel, A. Cambi, J. Greve, B. G. De Grooth, and C. G. Figdor. Biomolecular interactions measured by atomic force microscopy. *Biophys. J.* **79**:3267–3281 (2000).
30. M. Benoit, D. Gabriel, G. Gerisch, and H. E. Gaub. Discrete interactions in cell adhesion measured by single-molecule force spectroscopy. *Nat.Cell Biol.* **2**:313–317 (2000).
31. D. Leckband and J. Israelachvili. 2001. Intermolecular forces in biology. *Q. Rev. Biophys.* **32**:105–267 (2000).
32. J. Israelachvili. *Intermolecular & Surface Forces*. Academic, London, 1994, p. 200.
33. J. Israelachvili. *Intermolecular & Surface Forces*. Academic, London, 1994, p. 290.
34. T. W. G. Solomons and C. B. Fryhle. *Organic Chemistry*. Wiley, Hoboken, 2004, p. 510.
35. S. R. Goodman. *Medical Cell Biology*. Lippincott-Raven, New York, 1998, pp. 5–11.
36. T. W. G. Solomons and C. B. Fryhle. *Organic Chemistry*. Wiley, Hoboken, 2004, p. 673.
37. T. W. G. Solomons and C. B. Fryhle. *Organic Chemistry*. Wiley, Hoboken, 2004, p. 851.
38. T. W. G. Solomons and C. B. Fryhle. *Organic Chemistry*. Wiley, Hoboken, 2004, p. 982.
39. K. Troev. Dialkyl hydrogen phosphonates. 3. Reactions with the participation of the alpha-carbon atom of the alkoxy group. *Rev. Heteroatom Chem.* **11**:89–119 (1994).
40. K. Troev. Dialkyl hydrogen phosphonates.4. Addition Reactions. *Rev. Heteroatom Chem.* **12**:85–120 (1995).
41. T. W. G. Solomons and C. B. Fryhle. *Organic Chemistry*. Wiley, Hoboken, 2004, p. 854.
42. S. H. S. Leung and J. R. Robinson. J.R. Bioadhesive drug delivery. *ACS Sym.* **467**:350–366 (1991).
43. M. A. Burg, K. A. Grako, and W. B. Stallcup. Expression of the NG2 proteogylcan enhances the growth and metastatic properties of melanoma cells. *J. Cell. Physiol.* **177**:299–312 (1998).
44. A. G. de Galdeano, D. Boyano, I. Smith-Zubiaga, A. Alvarez, I. Canton, and L. Canavate. Involvement of interleukin-6 in the biology and metastatic activity of B16F10 melanoma cells. *Eur. Cytokine Netw.* **9**:187–192 (1998).
45. R. E. Eliaz and F. C. Szoka. Liposome-encapsulated doxorubicin targeted to CD44: a strategy to kill CD44-overexpressing tumor cells. *Cancer Res.* **61**:2592–2601 (2001).
46. D. Peer and R. Margalit. Tumor-targeted hyaluronan nanoliposomes increase the antitumor activity of liposomal doxorubicin in syngeneic and human xenograft mouse tumor models. *Neoplasia* **6**:343–353 (2004).
47. T. Hosooka, T. Noguchi, H. Nagai, T. Horikawa, T. Matozaki, M. Ichihashi, and M. Kasuga. Inhibition of the motility and growth of B16F10 mouse melanoma cells by dominant negative mutants of Dok-1. *Mol. Cell. Biol.* **21**:5437–5446 (2001).
48. T. W. G. Solomons and C. B. Fryhle. *Organic Chemistry*. Wiley, Hoboken, 2004, p. 832.
49. B. R. Line, A. Mitra, A. Nan, and H. Ghandehari. Targeting tumor angionesis: comparison of peptide and polymer-peptide conjugates. *J. Nuclear Medicine* **46**:1552–1560 (2005).
50. J. Hirabayashi, Y. Arata, K. Hayama, and K. Kasai. Galectins from the Nematode Caenorhabditis elagans and the Glycome Project. *Trends Glycosci. Glycotechnol.* **13**:533–549 (2001).
51. C. E. McNamee, Y. Tsujii, and M. Matsumoto. Interaction forces between two silica surfaces in an apolar solvent containing an anionic surfactant. *Langmuir* **20**:1791–1798 (2004).
52. J. Israelachvili. *Intermolecular & Surface Forces*. Academic, London, 1994, p. 31.
53. J. Israelachvili. *Intermolecular & Surface Forces*. Academic, London, 1994, p. 161.